Supporting Information

Patterned Surfaces for Solar Driven Interfacial Evaporation

Yini Luo, Benwei Fu, Qingchen Shen, Wei Hao, Jiale Xu, Mengdie Min, Yanming Liu, Shun An, Chengyi Song, Peng Tao, Jianbo Wu, Wen Shang, Tao Deng**

State Key Laboratory of Metal Matrix Composites, School of Materials Science and Engineering, Shanghai Jiao Tong University, 800 DongChuan Road, Shanghai 200240, P.R.China.

Corresponding author: dengtao@sjtu.edu.cn; shangwen@sjtu.edu.cn

Table of Contents

1. Supplementary Figures

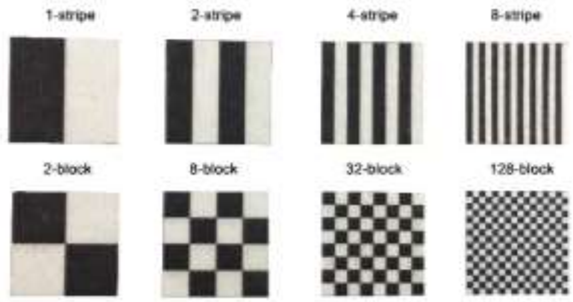

Figure S1. Photograph of printed patterns of stripes (the top row) and blocks (the bottom row) on the air-laid paper.

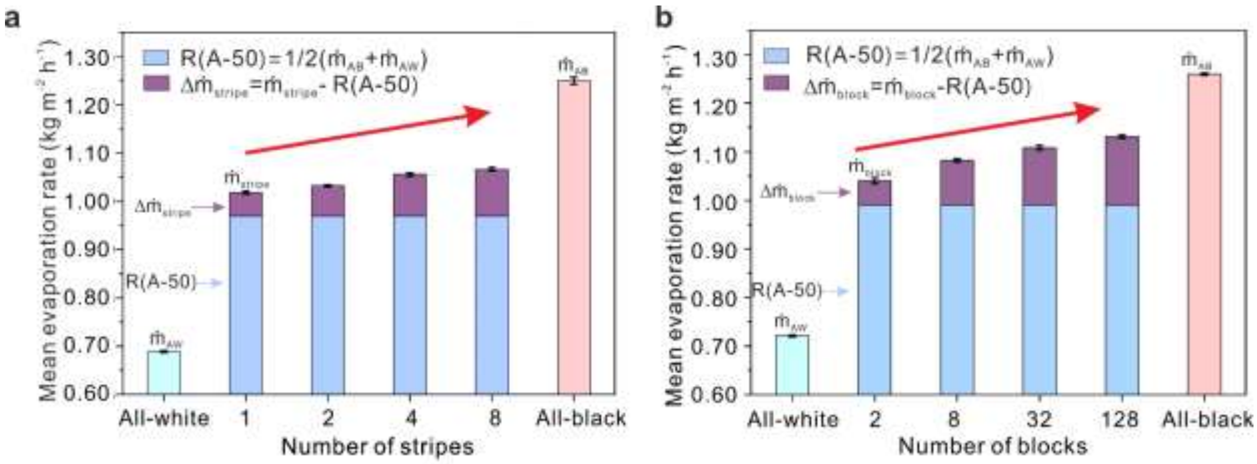

Figure S2. a) Comparison of evaporation rate of the four PAPs with different stripes in repeated operations. $\dot{m}_{AB}$ and $\dot{m}_{AW}$ represent the mean evaporation rate of AB and AW, respectively; $\dot{m}_{stripe}$ represents the mean evaporation rate of stripe patterns. b) Comparison of evaporation rate of the four PAPs with different blocks in repeated operations. $\dot{m}_{block}$ represents the mean evaporation rate of block patterns.

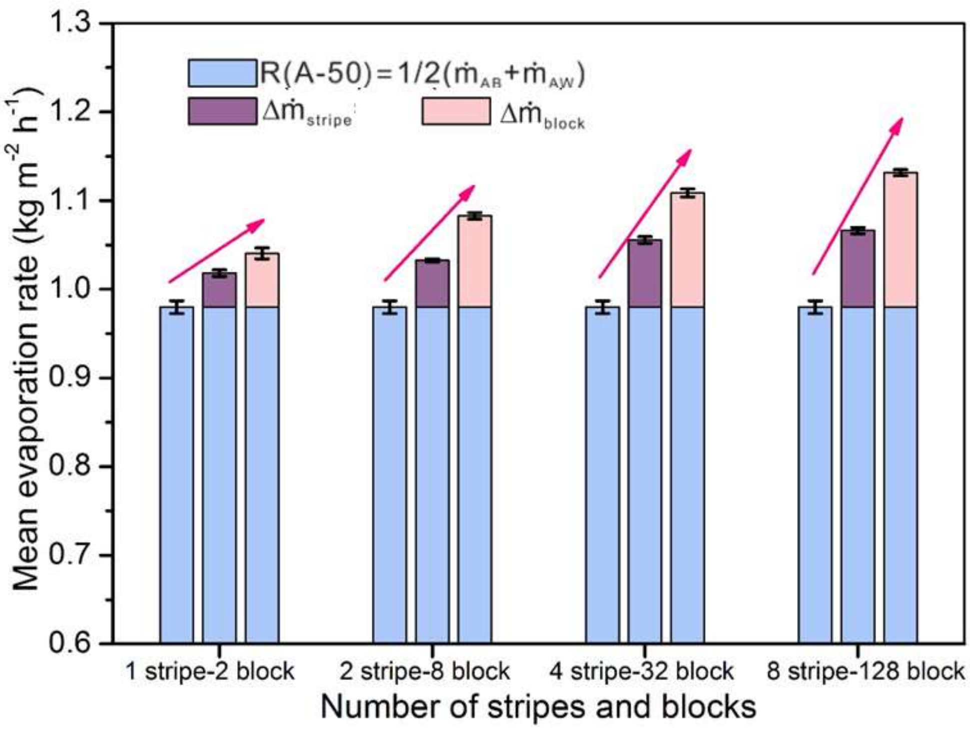

Figure S3. Comparison of evaporation rates of all PAPs with different stripes and different blocks in repeated operations. $\dot{m}_{AB}$ and $\dot{m}_{AW}$ represent the mean evaporation rate of AB and AW, respectively; $\Delta\dot{m}_{stripe}$ and $\Delta\dot{m}_{block}$ represent the evaporation enhancement of stripe patterns and block patterns, respectively.

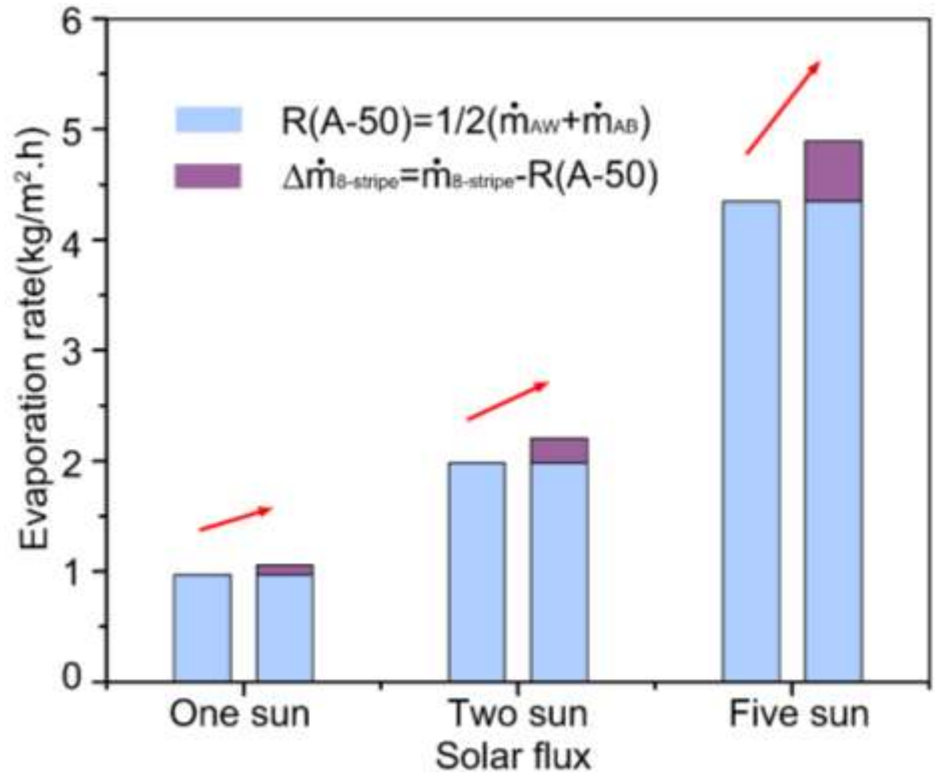

Figure S4. The evaporation rates of R(A-50) and the sample of 8-stripe under 1, 2, and 5 sun illumination for 30 min.

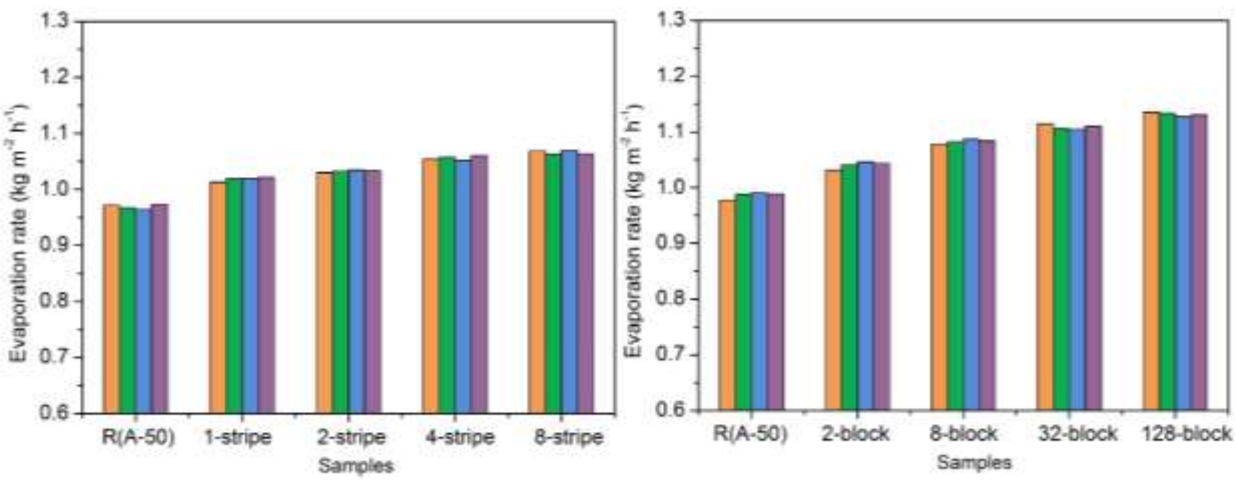

Figure S5. The evaporation rates for a) 1, 2, 4, 8-stripe samples, R(A-50), and b) 2, 8, 32, 128-block samples. Each sample was measured four times under the same condition exposed to 1 sun for 30 min.

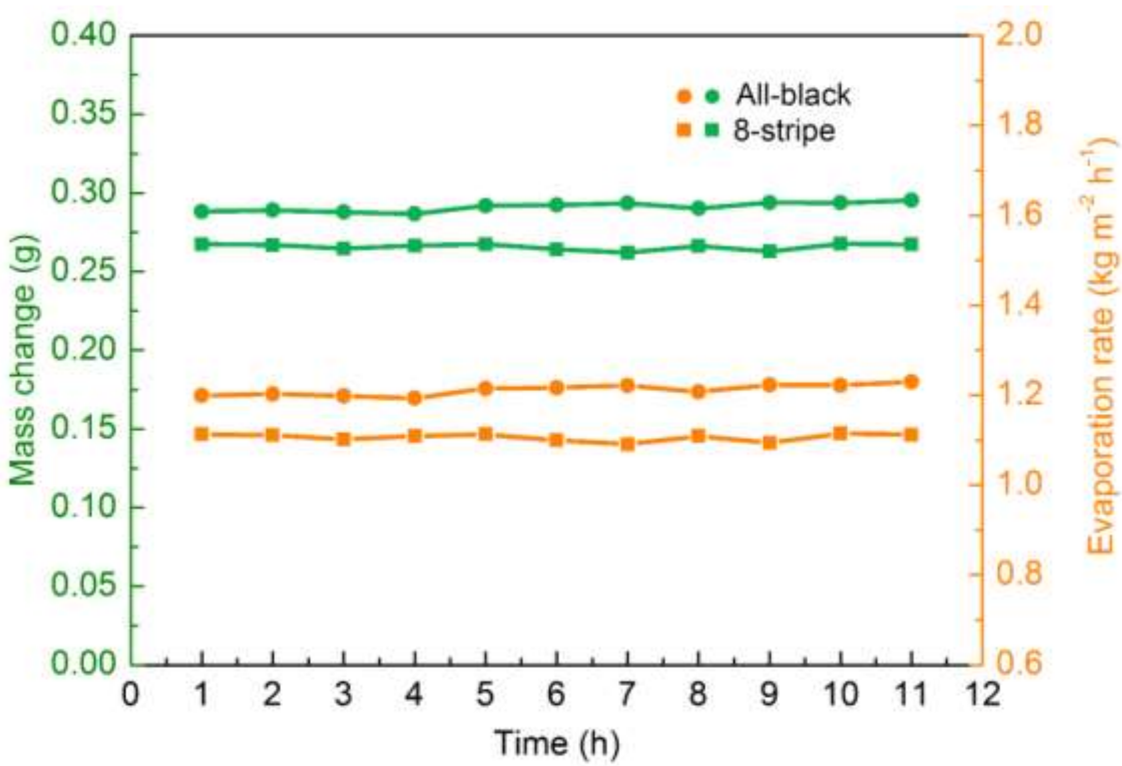

Figure S6. The mass change and evaporation rates for AB sample and 8-stripe sample at the surface of a simulated seawater (3.5 wt% NaCl solution) continuously exposed to 1 sun for 11 h.

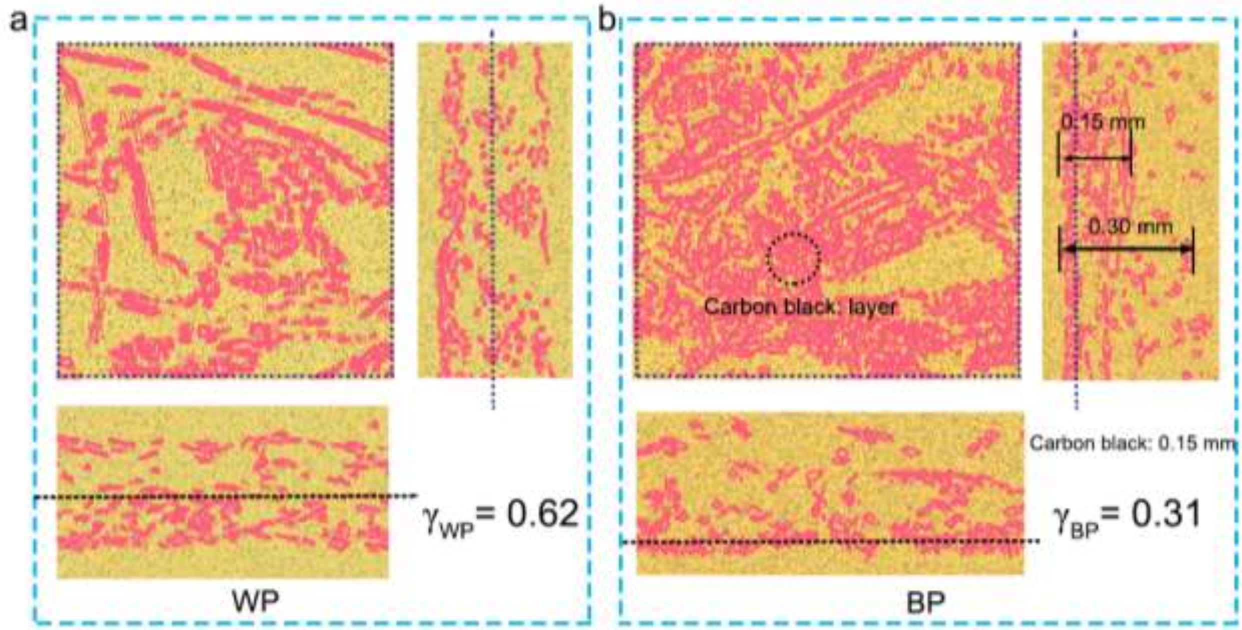

Figure S7.The cross section of printed air-laid paper at the area of a) WP and b) BP taken by Micro-CT. γ_{WP} and γ_{BP} represent the porosity of the WP and the BP.

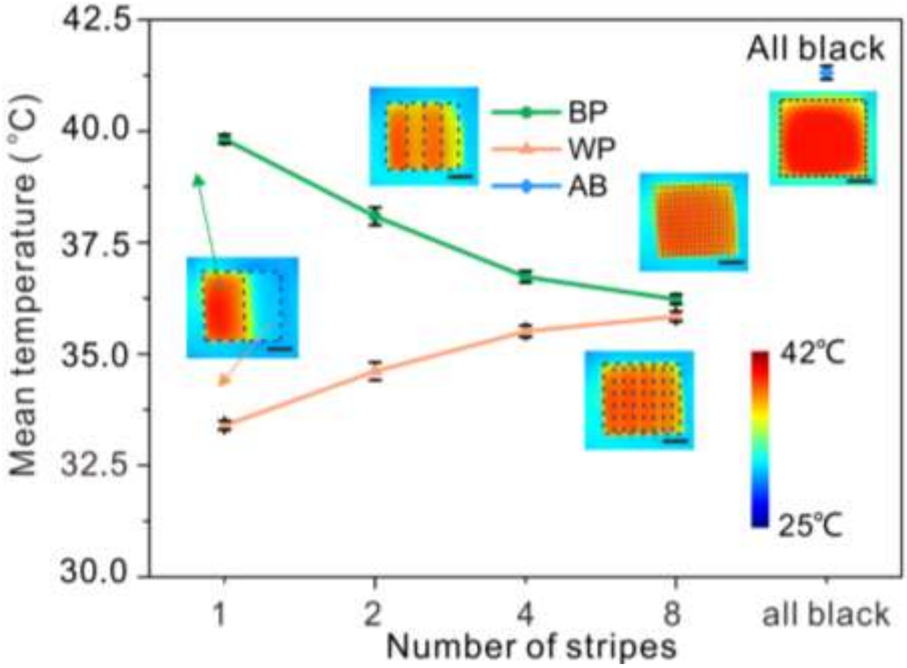

Figure S8. The temperature of the BP and the WP for 1, 2, 4, 8-stripe and all-black samples. Inserts are the infrared photographs of the 1, 2, 4, 8-stripe and all-black samples under one-sun illumination for 30 min, respectively. The black scale bars represent 5 mm.

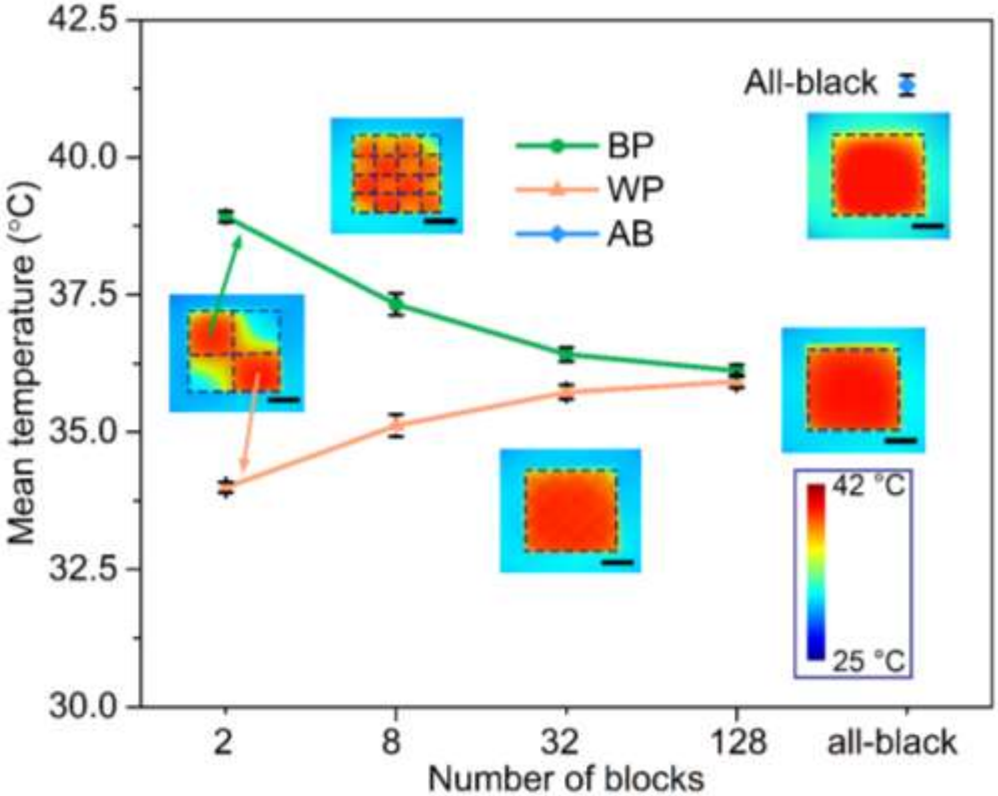

Figure S9. The temperature of the BP and the WP for 2, 8, 32, 128-block and all-black samples. Inserts are the infrared photographs of the 2, 8, 32, 128-block and all-black samples under one-sun illumination for 30 min, respectively. The black scale bar represents 5 mm.

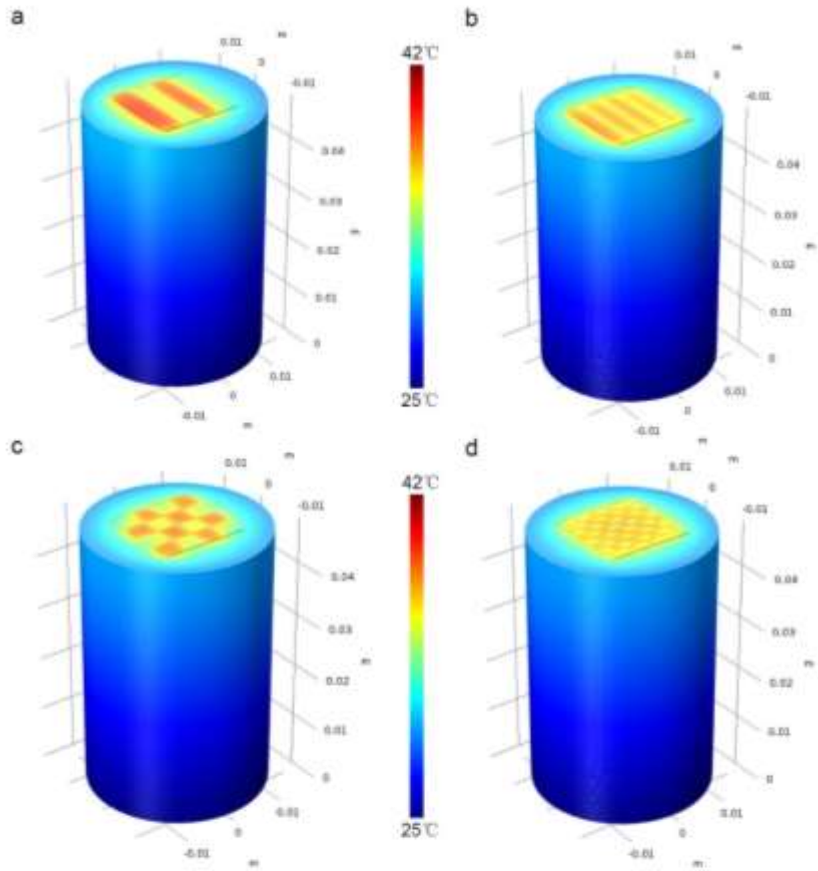

Figure S10. The distribution of surface temperature of the a) 2-stripe sample, b) 4-stripe sample, c) 8-block, and d) 128-block samples under one-sun illumination for 30 min, simulated using the COMSOL model.

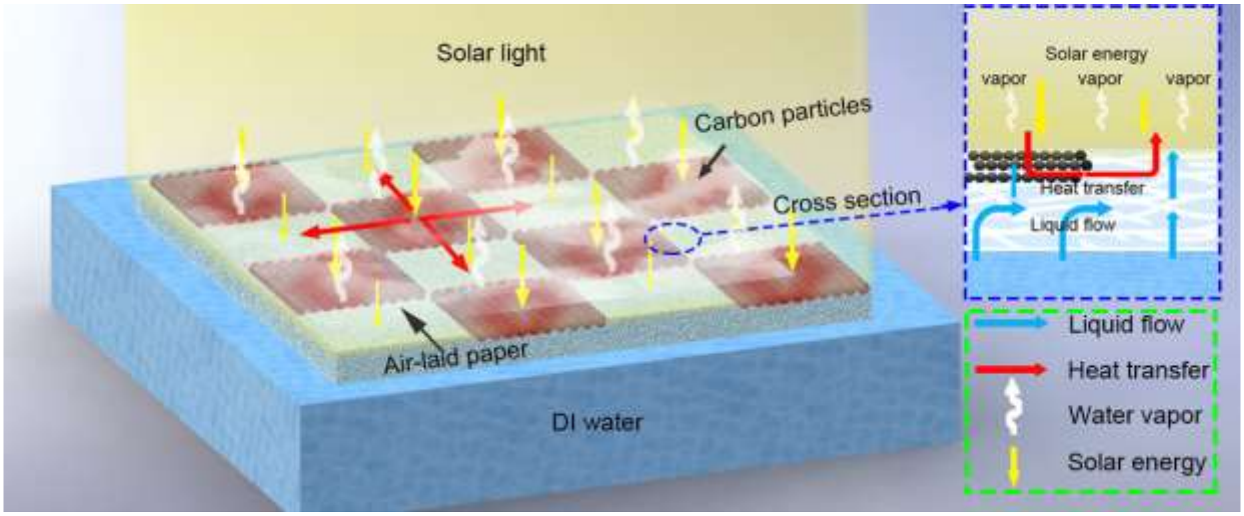

Figure S11. The schematic illustration of interfacial evaporation process on the surface of PAP with block-patterns under solar illumination. The insert shows the lateral heat and mass transfer between block patterns.

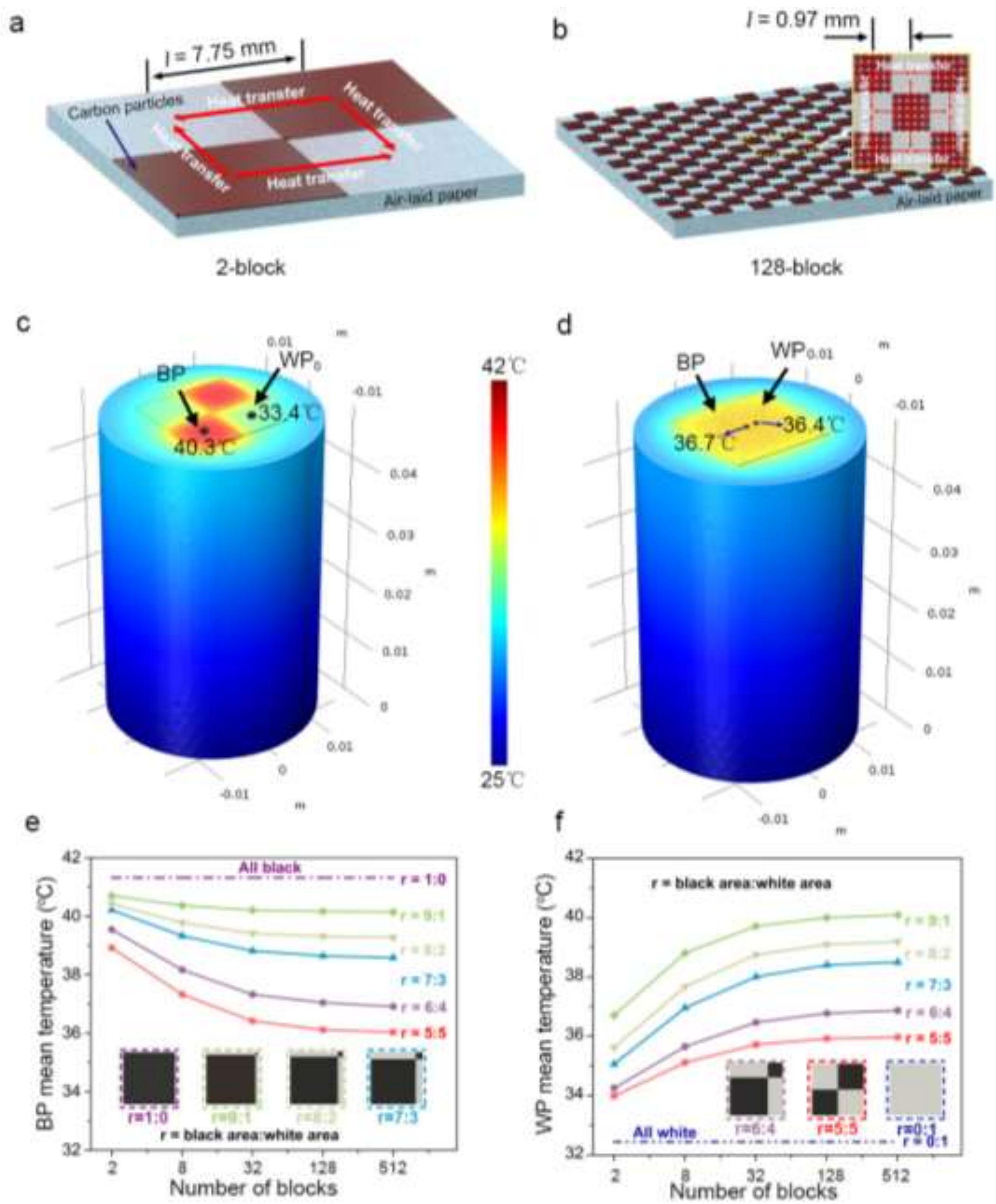

Figure S12. The schematic of the a) 2-block b) and 128-block samples under solar illumination. In (a) and (b), the black patterns represent carbon particles, and the white patterns represent the paper fibers. The red arrows represent the lateral heat transfer. c, d) A COMSOL model to simulate the distribution of temperature of the 2 and 128-block samples under one-sun illumination for 30 min, respectively. e) The simulated mean temperature of the BP with different r (r = black area: white area) for 2, 8, 32, 128, and 512-block samples. Inserts are schematics of 2-block sample with r = 1:0, 9:1, 8:2, and 7:3. f) The simulation of mean temperature of the WP with different r values for 2, 8, 32, 128, and 512-block samples. Inserts are schematics of 2-blocks with r = 6:4, 5:5, and 0:1.

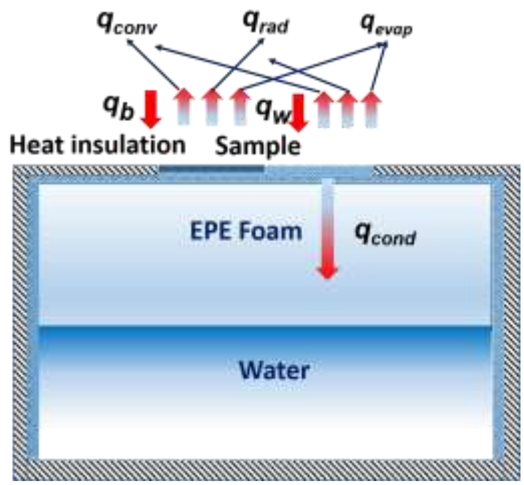

Figure S13. Energy balance and heat transfer diagram for a patterned absorber illuminated under one-sun.

2. Steady-state evaporation heat and mass transfer model:

2.1 The energy balance of the evaporation process and evaporation efficiency based on the analysis of heat loss

Mass changes and IR images of different samples were recorded when samples were illuminated by simulated solar light. In this work, a simple steady-state model is developed for analyzing the evaporation performance of PAP interfacial evaporation system. This model describes the working mechanism of the PAP evaporation system and the parameters that affect evaporation. A generic device comprising a solar absorber that transfers heat to water at the air-liquid surface and causes the water molecules to evaporate is shown schematically in **Figure S13**. In the model, we assume that the device is perfectly insulated on the bottom and side. The length and width of the sample are also assumed to be much larger than the thickness of the sample. So that all heat transfer processes in the sample are one-dimensional in the vertical direction.

The energy conversion equation can be expressed as

$$A_b q_b + A_w q_w = A_{total}(q_{rad} + q_{conv} + q_{cond} + q_{evap}), \tag{S1}$$

where, q_b and q_w are the absorbing heat flux of the BP and the WP, respectively; A_b and A_w are the area of the BP and WP, respectively; q_{rad} is the radiation heat loss of the absorber; q_{conv} is the convection heat loss of the absorber; q_{cond} represents the conduction heat loss from the EPE foam to the underlying water; q_{evap} is the heat flux for interfacial evaporation of the absorber. A_{total} is the total area of the absorber, $A_{total} = A_b + A_w$. q_b ,q_w , q_{rad}

q_{conv}, q_{cond} in Eq. (S1) can be expressed as

$$q_b = a_b q_s, \tag{S2}$$

$$q_w = a_w q_s, \tag{S3}$$

$$A_{total} q_{rad} = \varepsilon_b A_b \sigma\left({T_b}^4 - {T_\infty}^4\right) + \varepsilon_w A_w \sigma\left({T_w}^4 - {T_\infty}^4\right), \tag{S4}$$

$$A_{total} q_{conv} = h_{conv} A_b (T_b - T_\infty) + h_{conv} A_b (T_w - T_\infty), \tag{S5}$$

$$A_{total} q_{cond} = \frac{k_{EPE} A_{EPE}}{d_{EPE}}\left(T_{top} - T_{down}\right), \tag{S6}$$

where, q_s is the solar flux, 1000 W/m^2; α_b and α_w are the absorber absorption of the BP and WP, respectively; ε_b and ε_w are the emissivities of BP and WP, respectively; σ is the Stefan-Boltzmann constant, 5.67×10^{-8} W/(m^2 K^4); T_b and T_w represent the average surface temperature of the BP and the WP, respectively; T_∞ is the ambient temperature; h_{conv} is the convection heat transfer coefficient; k_{EPE} is the EPE foam thermal conductivity (~0.03 W/(m K)), and d_{EPE} is the EPE foam thickness (2.52 cm); A_{EPE} is the cross area of the EPE; T_{top} and T_{down} are the average temperatures for top and bottom surfaces of EPE, respectively. The evaporation efficiency η_h can be calculated using the following equation:

$$\eta_h = \frac{q_{evap}}{q_s} \cdot 100\% = \frac{A_b q_b + A_w q_w - A_{total}(q_{rad} + q_{conv} + q_{cond})}{A_{total} q_s}, \tag{S7}$$

In the Eq. (S1)-(S6), the unknown variables are T_b, T_w, T_{top}, and T_{down}. These unknown temperatures can be obtained from the experiment results. Based on the analysis of the heat loss, the evaporation efficiency of 1-stripe can be estimated to be 61.3%

2.2 Evaporation efficiency based on the analysis of mass flux

According to the calculated evaporation rate in the experiment, the heat flux for water evaporation q_m can be expressed as below:

$$q_m = mh_{lv} = cm(T_v - T_\infty) + m\Delta H, \tag{S8}$$

$$\eta_m = \frac{q_m}{q_s A_{total}}, \tag{S9}$$

where, m is the interfacial mass flux, h_{lv} is the total enthalpy of liquid-vapor phase change (sensible heat and latent heat), c is the specific heat capacity, T_v is the vapor temperature, T_∞ is the ambient temperature, ΔH is the phase-change enthalpy. Based on the analysis of mass flux, the evaporation efficiency of 1-stripe can be estimated to be 62.0%. The results derived from mass flux match well with these calculations derived from heat loss.

2.3 Lateral thermal conductivity

The effect of the stripe width (the stripe number) on the temperature of patterned surface and lateral thermal transfer, which can be analyzed by cross-section schematics as shown in Fig. 5a-b in the main text. The heat transfer process involves the heat conduction between the BP and WP. The heat conduction within the BP can be expressed as

$$q_{b,cond} = 1/R_b * (T_b - T_i), \tag{S10}$$

The heat conduction within the WP can be expressed as

$$q_{w,cond} = 1/R_w * (T_i - T_w), \tag{S11}$$

where, $q_{b,cond}$ and $q_{w,cond}$ are the conduction heat transfer of the BP and WP, R_b is the thermal resistance of the carbon black in the BP, R_w is the thermal resistance of the air-laid paper in the WP, T_b is the average temperature of the BP, T_i is the interfacial temperature between the BP and the WP, T_w is the average temperature of the WP. R_b and R_w can be expressed as,

$$R_b = l_b/(k_{b,eff} A_{cond}), \tag{S12}$$

$$R_w = l_w/(k_{w,eff} A_{cond}), \tag{S13}$$

where, l_b and l_w are the half width of the white and black stripe, respectively; $k_{b,eff}$ and $k_{w,eff}$ are the effective conductivity of the carbon black and air-laid paper, respectively; A_{cond} is the cross-sectional area of the stripe.

The effective thermal conductivity of the black and white porous wick can be expressed as [1]

$$\mathrm{k_{eff}} = \mathrm{k_f} * \frac{\mathrm{k_f} + \mathrm{k_s} - (1-\gamma) * (\mathrm{k_f} - \mathrm{k_s})}{\mathrm{k_f} + \mathrm{k_s} + (1-\gamma) * (\mathrm{k_f} - \mathrm{k_s})}, \tag{S14}$$

where, k_f is the thermal conductivity of the liquid (0.61 W m^{-1} k^{-1}), k_s is the thermal conductivity of the solid (air-laid paper: 0.03-0.05 W m^{-1} k^{-1}, carbon black: 0.30 W m^{-1} k^{-1})[2-3], γ denotes the porosity (air-laid paper: 0.62, carbon black: 0.31), According to the equation S14, we can calculate the $k_{b,eff}$ and $k_{w,eff}$.

3. References

1. Ma H. Oscillating Heat Pipes. *Springer New York*, **2015**.
2. Dominguez-Munoz, F.; Anderson, B.; Cejudo-Lopez, J. M.; Carrillo-Andres, A. Uncertainty in the Thermal Conductivity of Insulation Materials. *Energy Build.* **2010,** *42*, 2159-2168.
3. Khizhnyak, P.; Chechetkin, A.; Glybin, A. Thermal conductivity of carbon black. *J. Eng. Phys.* **1979**, *37*, 1073−1075.